Collective spin fluctuation mode and Raman scattering in superconducting cuprates

F. Venturini, Umberto Michelucci, T. P. Devereaux, Arno P. Kampf

Angaben zur Veröffentlichung / Publication details:

Venturini, F., Umberto Michelucci, T. P. Devereaux, and Arno P. Kampf. 2000. "Collective spin fluctuation mode and Raman scattering in superconducting cuprates." *Physical Review B* 62 (22): 15204–7. https://doi.org/10.1103/PhysRevB.62.15204.

Collective spin fluctuation mode and Raman scattering in superconducting cuprates

F. Venturini,[1] U. Michelucci,[2] T. P. Devereaux,[3] and A. P. Kampf[2]
[1]*Walther Meissner Institut, Bayerische Akademie der Wissenschaften, 85748 Garching, Germany*
[2]*Theoretische Physik III, Elektronische Korrelationen und Magnetismus, Institut für Physik, Universität Augsburg, 86135 Augsburg, Germany*
[3]*Department of Physics, University of Waterloo, Waterloo, ON, Canada N2L 3G1*
(Received 10 April 2000)

Although the low-frequency electronic Raman response in the superconducting state of the cuprates can be largely understood in terms of a *d*-wave energy gap, a long-standing problem has been an explanation for the spectra observed in the A_{1g} polarization orientations. We present calculations which suggest that the peak position of the observed A_{1g} spectra is due to a collective spin fluctuation mode.

Electronic Raman scattering has proven to be a useful tool in exploring the superconducting state in the cuprate materials. The possibility of probing selectively electronic excitations in different regions of the Brillouin zone (BZ) by the choice of polarization geometries has allowed us to explore the superconducting gap anisotropy. The successful explanation of the Raman data in B_{1g} and B_{2g} scattering geometries[1,2] has provided one piece of evidence for the by now widely accepted $d_{x^2-y^2}$ pairing symmetry in hole-doped cuprate superconductors.[3] In the context of impurity effects as a testing ground for unconventional superconductivity, the observed ω^3 to ω crossover in the low-frequency B_{1g} Raman response fits consistently with the power-law crossovers at low temperatures in the NMR relaxation rate and in the magnetic penetration depth. An even quantitatively consistent picture of electronic Raman scattering and infrared conductivity was achieved when the *T*-matrix approximation in the ''dirty'' *d*-wave scenario is extended to include a spatial extension of the impurity potential.[4]

However, up to now the discrepancy between Raman data in A_{1g} and B_{1g},B_{2g} geometries has remained unresolved.[5,6] Previous results for the A_{1g} scattering geometry were found to be very sensitive to changes in the Raman vertex function $\gamma(\mathbf{k})$[5] making a comprehensive explanation difficult for the experimental data in different cuprate materials.

In this paper we calculate the Raman response of a $d_{x^2-y^2}$ superconductor including the contribution from a collective spin-fluctuation (SF) mode which is identified with the (π,π,π)-resonance (in short π-resonance) near $\omega_R \approx 41$ meV observed by inelastic neutron scattering (INS) on bilayer cuprates.[7,8] Our results suggest that the A_{1g} peak position is largely controlled by the strength and frequency of the π-resonance mode which on the other hand does not affect the Raman response in the B_{1g} and B_{2g} channels. The inclusion of the collective SF mode allows for a simultaneous fit of the Raman data in all channels in optimally doped materials. Furthermore, we find that the inclusion of the SF term significantly reduces the sensitivity to the special choice of the underlying tight-binding band structure, i.e., the sensitivity to the choice of the Raman vertex in A_{1g} symmetry, and thus offers a possible route for resolving the previously encountered problems in the symmetry analysis of the light-scattering amplitude.[2,5]

On the basis of the observation of the collective SF mode in Y-123 and Bi-2212, we consider a bilayer model represented by a tight-binding band structure

$$\epsilon_{\mathbf{k}} = -2t[\cos(k_x)+\cos(k_y)] + 4t'\cos(k_x)\cos(k_y) - t_\perp(\mathbf{k}),$$

with an interplane hopping given by[9]

$$t_\perp(\mathbf{k}) = 2t_\perp\cos(k_z)[\cos(k_x)-\cos(k_y)]^2, \tag{1}$$

where k_z is 0 or π for the bonding or antibonding bands of the bilayer, respectively. Although there is no experimental evidence of the INS peak in the monolayer cuprates,[10] the results of this model are not qualitatively changed when a monolayer structure is considered.

The spin susceptibility (χ_s) is modeled by extending the weak-coupling form of a BCS superconductor in a $d_{x^2-y^2}$ pairing state to include antiferromagnetic spin fluctuations by a random-phase-approximation (RPA) form with an effective interaction $\bar{U}$; i.e., $\chi_s(\mathbf{q},i\omega) = \chi^0(\mathbf{q},i\omega)/[1-\bar{U}\chi^0(\mathbf{q},i\omega)]$ where[9]

$$\chi^0(\mathbf{q},i\omega) = \frac{1}{\beta}\mathrm{Tr}\sum_{\mathbf{k},i\omega'} \hat{G}(\mathbf{k},i\omega')\hat{G}(\mathbf{k}+\mathbf{q},i\omega'+i\omega). \tag{2}$$

Tr denotes the trace and $\beta = T^{-1}$. $\hat{G}(\mathbf{k},i\omega)$ is the BCS Green's function in Nambu space

$$\hat{G}(\mathbf{k},i\omega) = \frac{i\omega\hat{\tau}_0 + \xi_{\mathbf{k}}\hat{\tau}_3 + \Delta_{\mathbf{k}}\hat{\tau}_1}{(i\omega)^2 - \xi_{\mathbf{k}}^2 - \Delta_{\mathbf{k}}^2} \tag{3}$$

with $\hat{\tau}_i (i=1,2,3)$ being the Pauli matrices, $\hat{\tau}_0$ the 2×2 unit matrix, $\xi_{\mathbf{k}} = \epsilon_{\mathbf{k}} - \mu$, and $\Delta_{\mathbf{k}} = \Delta_0[\cos(k_x)-\cos(k_y)]/2$. This form of the spin susceptibility contains a strong magnetic resonance peak at $\mathbf{q} = \mathbf{Q} \equiv (\pi,\pi,\pi)$ which was proposed[9] to explain the INS resonance at energies near 41 meV in Y-123 (Ref. 8) and Bi-2212.[7] Other forms for the spin susceptibility can be straightforwardly used within our model. However, the results are mainly determined by the collective mode at $\mathbf{Q}$. Therefore, we take the bilayer susceptibility for a representative calculation.

The intensity of scattered light $I(\omega)$ in Raman experiments is proportional to the imaginary part of the response function for the effective density operator

$$\tilde{\rho}_{\mathbf{q}}=\sum_{\mathbf{k},\sigma}\gamma(\mathbf{k})c^{\dagger}_{\sigma,\mathbf{k}+\mathbf{q}}c_{\sigma,\mathbf{k}} \tag{4}$$

in the long-wavelength limit $\mathbf{q}\rightarrow 0$. Specifically

$$I(\Omega)\propto[1+n(\Omega)]\mathrm{Im}\chi(\Omega+i0^{+}),$$

$$\chi(i\Omega)=\int_0^{1/T}\mathrm{d}\tau\, e^{-i\Omega\tau}\langle T_{\tau}[\tilde{\rho}(\tau),\tilde{\rho}(0)]\rangle, \tag{5}$$

with the Bose function $n(\omega)$ and the time ordering operator T_{τ}.

The bare Raman vertex $\hat{\gamma}(\mathbf{k})=\hat{\tau}_3\gamma(\mathbf{k})$ in different scattering geometries are classified according to the elements of the D^{4h} point group. For the limiting case of vanishingly small scattered (ω_S) and incident (ω_I) photon energies, it can be represented in the effective-mass approximation (EMA)

$$\gamma(\mathbf{k})=\sum_{\alpha,\beta}e^{I}_{\alpha}\frac{\partial^2\epsilon_{\mathbf{k}}}{\partial k_{\alpha}\partial k_{\beta}}e^{S}_{\beta}, \tag{6}$$

where $\mathbf{e}^I$ and $\mathbf{e}^S$ are the unit vectors for in-plane polarizations (i.e., $\alpha,\beta\in\{x,y\}$) of the incoming and the scattered light, respectively. Using Eq. (6) and the bilayer tight-binding dispersion Eq. (1) we obtain

$$\gamma^{B_{1g}}_{\mathbf{k}}=2t\gamma^{d}_{\mathbf{k}}\left(1+\frac{4t_{\perp}}{t}\cos(k_z)[\cos(k_x)+\cos(k_y)]\right) \tag{7}$$

$$\gamma^{A_{1g}}_{\mathbf{k}}=2t\gamma^{s}_{\mathbf{k}}-2t_{\perp}\cos(k_z)[\cos(2k_x)+\cos(2k_y)] -4\cos(k_x)\cos(k_y)[t'+2t_{\perp}\cos(k_z)] \tag{8}$$

where $\gamma^{d,s}_{\mathbf{k}}=[\cos(k_x)\mp\cos(k_y)]/2$. However, the EMA has a questionable region of validity for all Raman measurements[5] on the cuprates since the incoming photons have energy ~ 2 eV, which is of the order of the bandwidth and of the interband excitations according to local density calculations.[11] EMA-based arguments in previous works about relative Raman intensities for different channels are therefore questionable.[6] We hence consider other forms for the vertices as well which obey the proper symmetry transformations. For the A_{1g} geometry some symmetry compatible choices are $\gamma(\mathbf{k})=\cos(k_x)+\cos(k_y)$ and $\gamma(\mathbf{k})=\cos(k_x)\cos(k_y)$. These basis functions assign weight to different regions of the BZ and this is the reason why previous results for the A_{1g} response were particularly sensitive to the specific choice of the bare Raman coupling vertex.

The spin fluctuations lead to an additional contribution for the Raman response via a two-magnon-like process as shown diagrammatically in Fig. 1.[12] Here, the SF propagator is incorporated in its RPA form for the bilayer (as described above) by the ladder diagram series with an effective on-site Hubbard interaction $\overline{U}$.

We, therefore, write the Raman response function at finite temperature as the sum of a pair-breaking (PB) and a SF contribution

$$\chi_{\gamma\gamma}(\mathbf{q},i\omega)=\chi^{PB}_{\gamma\gamma}(\mathbf{q},i\omega)+\chi^{SF}_{\gamma\gamma}(\mathbf{q},i\omega) \tag{9}$$

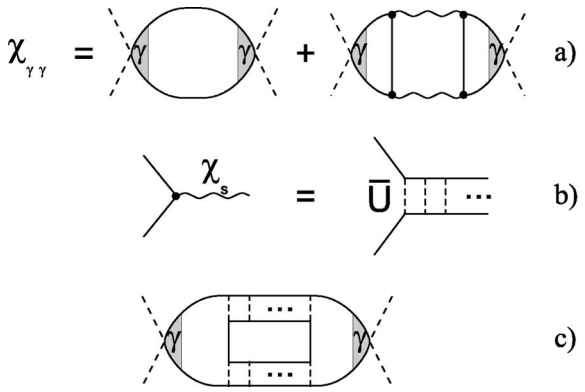

FIG. 1. (a) Feynman diagrams for the Raman response function including pair-breaking quasiparticle excitations and ''two-magnon processes.'' Dashed, wiggly, and solid lines represent photons, spin fluctuations, and fermionic propagators. γ denotes the bare Raman vertex in a selected scattering geometry. (b) Ladder series for the spin-fluctuation propagator. (c) Explicit diagram for the spin fluctuation contribution.

with the Raman vertex specifying the scattering geometry. In the limit $\mathbf{q}\rightarrow\mathbf{0}$ the diagram for the SF contribution translates into

$$\chi^{SF}_{\gamma\gamma}(i\Omega)=\frac{1}{\beta}\sum_{\mathbf{q}',i\omega}V^{\gamma}(\mathbf{q}',i\Omega,i\omega)\chi_s(-\mathbf{q}',-i\omega) \times\chi_s(\mathbf{q}',i\omega+i\Omega)V^{\gamma}(\mathbf{q}',-i\Omega,-i\omega). \tag{10}$$

The vertex function $V^{\gamma}(\mathbf{q}',i\Omega,i\omega)$ includes the bare Raman vertex and is evaluated as

$$V^{\gamma}(\mathbf{q}',i\Omega,i\omega)=\mathrm{Tr}\left\{\frac{1}{\beta}\sum_{\mathbf{k},i\omega'}\hat{\gamma}(\mathbf{k})\hat{G}(\mathbf{k},i\omega'+i\Omega) \times\hat{\tau}_0\overline{U}\hat{G}(\mathbf{k}+\mathbf{q}',i\omega'+i\Omega+i\omega) \times\hat{\tau}_0\overline{U}\hat{G}(\mathbf{k},i\omega')\right\}. \tag{11}$$

$i\Omega,i\omega$ denote bosonic and $i\omega'$ fermionic Matsubara frequencies. Similarly, $\chi^{PB}_{\gamma\gamma}$ is evaluated as

$$\chi^{PB}_{\gamma\gamma}(i\Omega)=\frac{\mathrm{Tr}}{\beta}\sum_{\mathbf{k},i\omega'}\hat{\gamma}(\mathbf{k})\hat{G}(\mathbf{k},i\omega')\hat{\gamma}(\mathbf{k})\hat{G}(\mathbf{k},i\omega'+i\Omega). \tag{12}$$

The total Raman response is calculated in the gauge-invariant form which results from taking into account the long-wavelength fluctuations of the order parameter to guarantee local charge conservation.[2,13] The total Raman susceptibility thus follows as

$$\chi(i\Omega)=\chi_{\gamma\gamma}(i\Omega)-\frac{\chi^2_{\gamma 1}(i\Omega)}{\chi_{11}(i\Omega)}, \tag{13}$$

where $\chi_{1\gamma}$ and χ_{11} are obtained by the replacement $\gamma(\mathbf{k})\rightarrow 1$ in one or both bare Raman vertices in the vertex function Eq. (11). The analytical continuation to the real axis is performed using Padé approximants.[14]

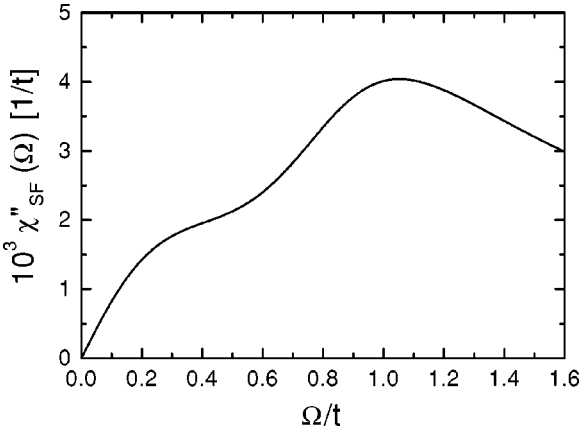

FIG. 2. ''Two-magnon process'' contribution $\chi^{SF}_{\gamma\gamma}$ in the A_{1g} geometry. The parameters used are defined in the text.

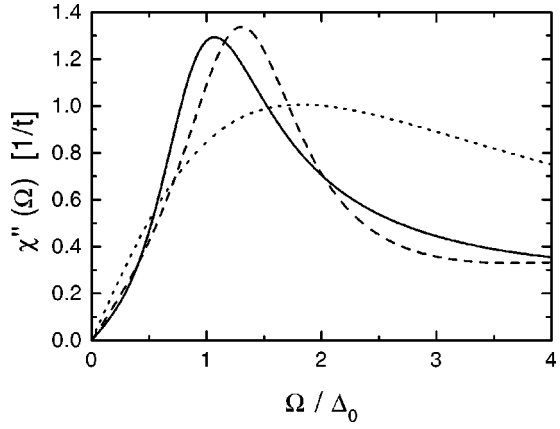

FIG. 3. The total response in the A_{1g} channel. Solid, dashed, and dotted lines correspond to $\bar{U}=0$, $\bar{U}/t=1.3$, and $\bar{U}/t=2.0$ respectively.

The band-structure parameters are chosen for all the numerical calculations to be applicable to optimally doped systems: $\langle n\rangle=0.85$, $t'/t=0.45$, $t_\perp/t=0.1$,[5] while the gap has been chosen as $\Delta_0/t=0.25$. The effective interaction $\bar{U}$ and the hopping integral t are used as the only two fit parameters, as explained below. The Raman response is evaluated at the fixed temperature $T/t=0.08$.

Let us first consider χ_{SF} alone. In Fig. 2 we plot χ''_{SF} for the A_{1g} channel versus frequency. χ_{SF} is the convolution of two spin susceptibilities [see Eq. (10)] and therefore has a maximum near twice the magnetic resonance frequencies in $\mathrm{Im}\chi_s(\mathbf{q},\omega)$ at $\mathbf{q}=\mathbf{Q}$ and $\mathbf{q}=\mathbf{Q}'=(\pi,\pi,0)$. For the chosen parameters $\mathrm{Im}\chi_s$ has a strong peak for $\mathbf{q}=\mathbf{Q}$ near $\omega_R\approx 0.4$ and a weaker peak for $\mathbf{q}=\mathbf{Q}'$ at a slightly higher frequency; we note that ω_R and the peak frequency in $\mathrm{Im}\chi_{SF}$ scale linearly with Δ_0. An important point is that in the B_{1g} and B_{2g} geometries the SF term introduces vanishingly small corrections to the total response, rendering the presence of the SF term important only in the A_{1g} geometry. This is due to the sharpness in momentum space of the resonance peak at $\mathbf{Q}$ in the SF propagator. In fact, if the transfer is taken only at $\mathbf{Q}$, both the B_{1g} and B_{2g} contributions to χ_{SF} vanish identically, as can be seen from Eq. (11). Therefore, for these channels the response is given by the PB term alone.

In Fig. 3 we illustrate the frequency dependence of $\chi''(\Omega)$ in the A_{1g} geometry for three different values of the effective interaction with both the PB and SF contributions included. The shape of the Raman response is modified varying $\bar{U}/t$ and in particular the position of the resonance is shifted towards higher energies for increasing $\bar{U}$. With the inclusion of the SF term we now obtain a peak slightly above Δ_0 as observed experimentally in Y-123 and Bi-2212.

A comment is in order on the relative magnitude of the SF and the PB term. Comparing Figs. 2 and 3 it is clear that the SF term is much smaller than the PB term, but the effect of this new term is nevertheless visible since the backflow [the second term in Eq. (13)] mixes in a nontrivial way the two contributions. Since the SF term varies as $\bar{U}^4$ in our model it starts to dominate for larger $\bar{U}$, leading to a shift in spectral weight out towards $2\omega_R$, which also changes with $\bar{U}$.

The experimental position of the peak is not sample dependent in the A_{1g} geometry as already mentioned, and is almost the same in different cuprates. On the other hand, the theoretical description with the PB term alone is very sensitive to Raman vertex changes, which can produce variation of its position between Δ_0 and $2\Delta_0$,[5] not allowing for a comprehensive modeling of different cuprates.

In Fig. 4 we address the problem of the sensitivity of the result to changes in the bare Raman vertex $\gamma(\mathbf{k})$. To investigate the effect of changes of the vertex function, we have calculated the final response using the three different forms for the vertex $\gamma(\mathbf{k})=\cos(k_x)+\cos(k_y)$, $\gamma(\mathbf{k})=\cos(k_x)\cos(k_y)$

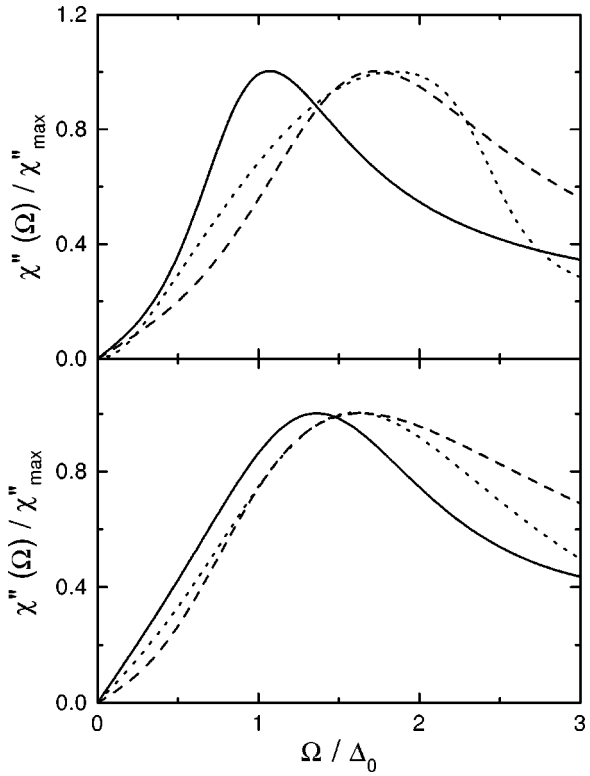

FIG. 4. The total A_{1g} response for different vertices: γ obtained from effective mass approximation (solid line), $\cos(k_x)+\cos(k_y)$ (dashed line), $\cos(k_x)\cos(k_y)$ (dotted line). In the upper panel the Raman response is plotted for $\bar{U}=0$, in the lower panel for $\bar{U}/t=1.3$.

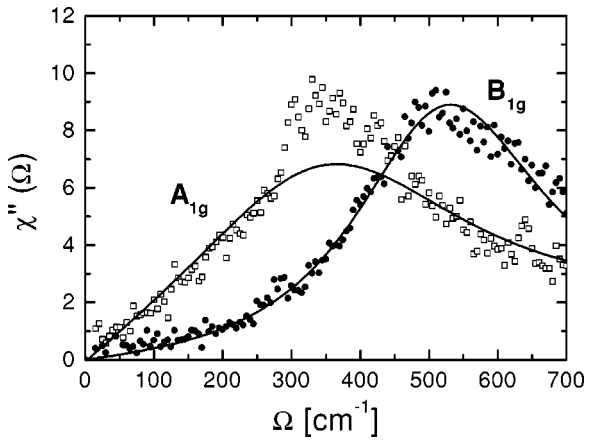

FIG. 5. Comparison of the A_{1g} and B_{1g} response with Bi-2212 data. The parameters used are $t'/t=0.45, t=130$ meV, $\Delta_0/t=0.25, \bar{U}/t=1.3$, and $\langle n\rangle=0.85$.

and in the EMA which posses the correct transformation properties required by symmetry. All curves are renormalized to their peak height to allow for an easier comparison. Clearly the strong sensitivity to changes of the bare Raman vertex (first panel) is much reduced when the SF term is added (second panel). As we have verified in detail, this reduced sensitivity is not altered by different model parameter choices and different broadening of the response.

In Fig. 5 we compare the theoretical results with experimental data on optimally doped Bi-2212.[5] Adding the SF contribution leads to a shift of the peak position from near $\sim\Delta_0$ for $\bar{U}=0$ to higher frequencies, and thus to a better agreement with the experimental relative peak positions in A_{1g} and B_{1g} geometries. For the fit we have adjusted t to achieve a good agreement with the B_{1g} channel, and then adjusted $\bar{U}$ to match the A_{1g} peak position.

The value of t obtained from the fit is $t=130$ meV. This value has to be compared with $t\approx 105$ meV, which results from the condition $\omega_R\approx 40$ meV. This slight discrepancy is most probably related to our simple modeling of the propagators which neglects strong renormalizations from interactions as well as impurities. We note that the excess intensity in the A_{1g} channel (see Fig. 5) above the theory line is somewhat sample dependent and is possibly related to disorder-induced effects of phonons.[15,16]

From this work we conclude that including the SF contribution in the Raman response solves the previously unexplained sensitivity of the A_{1g} response to small changes in the Raman vertex. Also, within our model it is now possible to obtain the correct relative peak positions of the A_{1g} and the B_{1g} scattering geometry. Whereas the SF (two-magnon) contribution controls the A_{1g} peak, the B_{1g} and B_{2g} scattering geometries are essentially unaffected and determined by pair-breaking processes alone.

We would like to thank R. Hackl for numerous discussions. F.V. would like to thank the Gottlieb Daimler and Karl Benz Foundation for financial support. This work was partially supported by the Deutsche Forschungsgemeinschaft through SFB 484.

[1] T.P. Devereaux, D. Einzel, B. Stadlober, R. Hackl, D.H. Leach, and J.J. Neumeier, Phys. Rev. Lett. **72**, 396 (1994).

[2] T.P. Devereaux and D. Einzel, Phys. Rev. B **51**, 16 336 (1995); **54**, 15 547 (1996).

[3] J. Annett, N. Goldenfeld, and A.J. Leggett, in *Physical Properties of High Temperature Superconductors*, edited by D. M. Ginsberg (World Scientific, Singapore, 1996), Vol. 5.

[4] T.P. Devereaux and A.P. Kampf, Phys. Rev. B **59**, 6411 (1999).

[5] T.P. Devereaux, A. Virosztek, and A. Zawadowski, Phys. Rev. B **54**, 12 523 (1996).

[6] F. Wenger and M. Käll, Phys. Rev. B **55**, 97 (1997); T. Strohm and M. Cardona, *ibid.* **55**, 12 725 (1997); **58**, 8839 (1998); D. Manske, C. Rieck, R. Das Sharma, A. Bock, and D. Fay, *ibid.* **56**, R2940 (1997); **58**, 8841 (1998); A.V. Chubukov, D.K. Moor, and G. Blumberg, Solid State Commun. **112**, 183 (1999).

[7] H.F. Fong, B. Keimer, P.W. Anderson, D. Reznik, F. Dogan, and I.A. Aksay, Phys. Rev. Lett. **75**, 316 (1995); H.F. Fong, P. Bourges, Y. Siddis, L.P. Regnault, A. Ivanov, G.D. Gu, N. Koshizuka, and B. Keimer, Nature (London) **398**, 588 (1999).

[8] H.A. Mook, M. Yethiraj, G. Aeppli, T.E. Mason, and T. Armstrong, Phys. Rev. Lett. **70**, 3490 (1993).

[9] N. Bulut and D.J. Scalapino, Phys. Rev. B **53**, 5149 (1996).

[10] T.E. Mason, *Handbook on the Physics and Chemistry of Rare Earths*, edited by K.A. Gschneider Jr., L. Eyring and M.B. Maple (Elsevier, Amsterdam, 1997), Vol. 24.

[11] O.K. Andersen, O. Jepsen, A.I. Liechtenstein, and I.I. Mazin, Phys. Rev. B **49**, 4145 (1994).

[12] A.P. Kampf and W. Brenig, Z. Phys. B: Condens. Matter **89**, 313 (1992).

[13] Note that the term ''screening'' has been used to describe the backflow yielding the second term in Eq. (13). However, the backflow is independent of the charge of the carriers and comes into play solely from the pair interactions responsible for superconductivity. It yields the well-known Anderson-Bogoliubov mode which restores gauge invariance. Details can be found in Ref. 2.

[14] H.J. Vidberg and J.W. Serene, J. Low Temp. Phys. **29**, 179 (1977).

[15] R. Hackl (private communication).

[16] The A_{1g} symmetry is not directly observable in tetragonal systems but is obtained by subtraction of two measured symmetries (e.g., $xx-x'x'$). However, each of the two measured spectra contains phonons of the corresponding symmetry, which have to be subtracted, too, to extract the electronic contribution. It is, therefore, possible that disorder-induced effects of phonons are not completely subtractable and produce the additional spectral weight.